Molecular orbital analysis of selected organic p-type and n-type conducting small molecules

Denisa Cagardová, Vladimír Lukeš

Department of Chemical Physics, Slovak University of Technology in Bratislava, Radlinského 9, SK-812 37 Bratislava, Slovakia
xcagardova@is.stuba.sk

Abstract: In this article, the selected series of commercially available p-type and n-type semiconducting small molecules are systematically studied by density functional theory using the B3LYP hybrid functional and 6-311G(2d,p) basis set. The optimal geometries of each molecule in the electronic neutral and corresponding charged states are calculated. The evaluated energies of frontier molecular orbitals and electronic band gaps are mutually compared together with adiabatic electronic intramolecular reorganization energies. The chemical accuracy of the evaluated theoretical quantities is estimated from the comparison with available experimental data.

Keywords: Aromatic structure; chemical structure; electron structure; molecular orbital; reorganization energy

Introduction

Organic semiconductors are mostly π-conjugated polycyclic and heterocyclic systems which have a certain degree of electrical conductivity. There are two major classes of organic semiconductors: low-molecular-weight materials and polymers (Zahn et al., 2006). Both of them have in common a conjugated p-electron system formed by the p_z orbitals of the sp^2-hybridized carbon atoms in the molecules. In comparison to the σ bonds constituting the backbone of the molecules, π bonding is significantly weaker. Therefore, the lowest electronic excitations of conjugated molecules are the π—π transitions with an energy gap typically between 1.5 and 3.0 eV leading to the light absorption or emission in the visible spectral range (Sawadogo et al., 2016). In detail, the electronic properties of a molecule depend on factors such as conjugation length or the presence of electron donating or withdrawing groups. Thus organic chemistry offers a wide range of possibilities to tune the optoelectronic properties of organic semiconducting materials (Brütting, 2005).

The electrical conductivity, as the macroscopic quantity, is extrinsic and it may have an origin in the delocalization of π-electrons or in the movement of charge defects generated by redox reactions under an electric field (Sawadogo et al., 2016). Structural and morphological studies have shown the dependence of molecular packing on the electrical conductivity due to its effect on charge mobility. For example, the thiophene or phenyl units in oligomers or polymers were found to give more planar structures, increase in the π-bonds conjugation and better π-electrons delocalization. Organic semiconductors can be divided according to the character of charge carriers into p-type (a positive charge or hole as the major carrier), n-type (a negative charge or electron as the major carrier) or ambipolar organic semiconductors (both electrons and holes are involved as charge carriers) (Cornill et al., 2007). The p-type conductivity was observed for the fused-ring arene compounds, including oligoacenes, and their derivatives (Filo and Putala, 2010). Special attention has been given to the pentacene molecule and its soluble derivatives. Another interesting class of p-type semiconductors are oligothiophenes or aromatic heterocycles containing sulphur atoms. An effective approach for n-type organic semiconductors is to convert known p-type materials into the n-type ones by modifying them with strongly electronegative fluorine atoms (Filo and Putala, 2010). No matter the position or the type of electron-withdrawing substitution, perfluorarene and perfluoroalkyl both greatly affect the crystal structure and charge transport. Arene-tetracarboxylic diimides represent another group of electron-deficient π-systems suitable for producing n-type semiconductors. They exhibit relatively high electron affinities, high electron mobilities and excellent chemical, thermal and photochemical stabilities. Widely used rylene diimides include naphthalene diimides and perylene diimides. The key factors, which affect the electronic structure of molecules and their charge injection and charge transport abilities, are molecular energy gaps and energy levels. These quantities can be determined experimentally (Reiss et al., 2011) or theoretically.

The Density functional theory (DFT) and time-dependent DFT (TD-DFT) are the first-principle approaches for orbital energy modelling of conjugated systems with a moderate computational cost

(Hohenberg and Kohn, 1964; Runge and Gross, 1984). The DFT method is convenient for the gas-phase optimal geometry investigation of large molecules because it includes effects of electron correlation. At the first approximation level, the vertical band gaps can be evaluated as the difference of the Kohn-Sham energies of the highest occupied molecular orbital (HOMO) and the lowest unoccupied molecular orbital (LUMO). On the other hand, the adiabatic geometrical changes upon the electric charging can be theoretically estimated from the reorganization energies $\lambda^{\pm}$ which are associated with the intermolecular electron transfer reaction (Olivier et al., 2006). The hybrid DFT functional such as B3LYP is popular to yield reasonably accurate ground and excited state energies of many conjugated systems (McCormick et al., 2013) what affects directly the evaluation of reorganization energies.

Although during the last two decades a large number of theoretical studies of various small organic molecules were published (Sigma Aldrich, 2017), the systematic comparisons of the vertical band gaps with respect to the adiabatic reorganization energies and molecular structure of typical p-type and n-type conducting molecules are not available. With respect to this fact, we decided to present the theoretical study of selected small organic molecules (Figs. 1 and 2) which are used in electronics industry. The partial aims of this study are: (1) to calculate the optimal geometries of the electric neutral, cationic and anionic charged states; (2) to evaluate the energies of frontier molecular orbitals and (3) to calculate the reorganization energies using the density functional theory. The evaluated quantities will be mutually compared and correlated with experimentally available data.

Computational details

The quantum chemical calculations were performed using Gaussian 09 program package (Frisch et al., 2010). The optimal geometries of studied molecules in the electronic neutral and anionic form were calculated in water by DFT method with B3LYP (Becke's three parameter Lee–Yang–Parr) functional (Lee et al., 1988; Becke, 1988) without any constraints (energy cut-off of 10^{-5} kJ×mol^{-1}, final RMS energy gradient under 0.01 kJ×mol^{-1}×A^{-1}). For all calculations, 6-311G(2d,p) basis sets were employed for all atoms (Hariharan and Pople, 1973; Rassolov et al., 1998). The optimized structures were confirmed to be real energy minima by vibrational analysis (no imaginary frequencies). The calculated molecules were visualised using the Molekel program package (Flukiger et al., 2002).

The reorganization energy is usually described as the sum of internal and external contributions. The internal reorganization energy refers to the energy required for the geometry relaxation when going from the neutral state to a charged molecular state and vice versa. This energy (Marcus, 1993; Brédas et al., 2004; Wang et al., 2014) is obtained from the adiabatic potential energy surfaces (PES) method as

$$\lambda^{\pm} = \lambda_1^{\pm} + \lambda_2^{\pm} = \left[E_{\pm}(Q_N) - E_{\pm}(Q_{\pm})\right] + \left[E_N(Q_{\pm}) - E_N(Q_N)\right] \quad (1)$$

where $E_{\pm}(Q_N)$ is the total energy of the charged state in the neutral geometry, $E_{\pm}(Q_{\pm})$ is the total energy of the charged state in the charged state geometry, $E_N(Q_{\pm})$ is the total energy of the neutral state in the charged state geometry, and $E_N(Q_N)$ is the total energy of the neutral state in the neutral geometry. Reorganization energy $\lambda^{\pm}$ includes contributions of relaxation energies $\lambda_i^{\pm}$. The energy difference between charged state in its equilibrium (neutral) geometry and in the relaxed (ion) geometry is characterised by the relaxation energy $\lambda_1^{\pm}$. The relaxation energy $\lambda_2^{\pm}$ has been determined by the difference between energy of neutral geometry in its equilibrium state and in relaxed state of molecule. In the case of cationic form of ion, we obtain the reorganization energy for hole. If ion was created by the reduction of molecule to the anionic form, contributions of relaxation energies resulted in reorganization energy for electron. The contribution to the $\lambda^{\pm}$ energy for both types of molecules is quite small and is of the order of a few tenths of an electron volt (Yin et al., 2006; Norton and Brédas, 2008).The small difference between the structures of the two compounds leads to the large difference between their reorganization energies.

Results and Discussion

The B3LYP optimal geometries of the molecules with the condensed aromatic rings are planar. The side addition of the phenyl moieties to the planar skeleton leads to the perpendicular or quasi-perpendicular orientation of **III-p**, **IV-n**, **XI-n** and **XII-n** molecules (see Fig. 3). The similar molecular structure was obtained for **VIII-n** molecule where two cyclohexyl rings with the chair-type conformations are directly connected with the nitrogen atoms. Next, the connection of the thiophene or phenyl rings to the heteroaromatic ring via α-positions is responsible for the relatively small planarity changes. The dihedral angle torsion between the neighbouring aromatic moieties is of approximately 24° for **IV-p**, nearly 28.5° for **X-p**,

26° for **XI-p**, 22° between two thiophene rings and 27° between thiophene and phenyl ring for **XII-p**, 39° for **XIV-p** and **V-n** is practically planar (Fig. 3). In the case of more possible conformations, the subsequent calculations analyses were performed for the most energetically preferred structure. For example, the *all-trans* conformations were used for quarterthiophene denoted as **IV-p**, sexithiophene **V-p**, 5,5'-di(4-biphenylyl)-2,2'-bithiophene **XII-p** and 2,2'-bis[4-(trifluoromethyl)phenyl]-5,5'-bithiazole **V-n**.

The electric conductivity, i.e. the charge flux in semiconducting materials, is very often explained using the analysis of frontier molecular orbitals with the particular reference to the HOMO-LUMO energy gaps. The efficient charge transport is mainly attributed to π-system extending with strong intermolecular overlaps. The optimal interval of energy level of the highest occupied orbitals for typical p-type semiconducting molecules is from 4.9 to 5.5 eV (Filo and Putala, 2010), because standard metallic hole injecting electrodes have comparable ionisation potentials, e.g. 5.1 eV below the vacuum level for Au. On the other hand, n-type dopants have a LUMO energy level between ca 3.0 and 4.0 eV (Filo and Putala, 2010).

For selected small p-type molecules, the gas-phase HOMO energies ranged from –4.65 to –5.60 eV and the LUMO energy levels are between –1.12 and –3.57 eV (see Fig. 4). The corresponding HOMO-LUMO ΔE_g gaps are changed from 2.01 to 3.86 eV. The mutual comparison of **I-p**, **II-p** and **III-p** illustrates how the elongation of acene centre and the addition of side phenyl rings are able to decrease the ΔE_g differences. On the other hand, the anthra[2,3-b:6,7-b']dithiophene molecule denoted as **IX-p**, in comparison to the pentacene (**II-p**) exhibits by about 0.5 eV larger ΔE_g gap. It seems that the presence of sulphur atoms decreases LUMO energy levels and increase HOMO energy levels, what is the direct consequence of the extension of the energy gap ΔE_g. The lowest ΔE_g value exhibits **X-p** compound where the polycondensed heteroaromatic structure is combined with phenyl rings. The inspection of Fig. 4b (n-type semiconducting organic molecules) shows that the gas-phase HOMO energies ranged from –4.26 to –7.87 eV and the LUMO energies are between –0.20 and –5.41 eV. The significantly lower LUMO energy levels have the quinoide structures **I-n** and **II-n** which consist of strong electron withdrawing cyano groups. The molecule denoted as **II-n** has the lower LUMO energy level in comparison with **I-n** due to further withdrawing fluorine atoms. The lowest ΔE_g value (0.90 eV) has **VIII-n** molecule with two chair-type conformations of cyclohexyl rings directly connected to nitrogen atoms. The largest studied 3D-spaced molecule is fullerene C_{60} (**XIII-n**) which represents an important n-type organic semiconductor. According to the next theoretical calculations (Beu et al., 2005), this molecule exhibits a relatively low lying LUMO energy level (–3.46 eV) that is triply degenerate. The reliability of the calculated B3LYP energies of frontier orbitals can be estimated by the comparison with the experimental data (Sigma Aldrich, 2017) obtained from the spectroelectrochemical measurements in solvents. These values are presented in parentheses in Fig. 4. Although the maximal difference between the gas-phase theoretical and experimental energies is of 0.3 eV, the general trends are correctly estimated. Table 1 summarizes evaluated relaxation and reorganization energies of a hole and electron. The largest reorganization energy of the hole was found for **VII-p** (0.513 eV) while the lowest value (0.099 eV) has **IX-p** molecule. In the case of the electron reorganization energies, by about 30 % larger values were obtained. The maximal electron reorganization energy has the **VIII-n** molecule (1.357 eV) and the minimal one (0.228 eV) exhibits the largest planar studied molecule, derivative of bisbenzimidazole, denoted as **IX-n**.

Conclusions

In this work, we investigated the selected series of commercially available small p-type and n-type semiconducting molecules systematically, that means through the same approach with the identical B3LYP hybrid functional and 6-311G(2d,p) basis sets. The main contribution of the article is the general summary of electrical properties like energy levels of frontier molecular orbitals (HOMO and LUMO), energy gaps and reorganization energies (for hole and electron) with contributions of corresponding relaxation energies. The optimal geometries of each molecule in the electronic neutral and the corresponding charged states were also calculated by density functional theory at the B3LYP/6-311G(2d,p) level of theory. The evaluated energies of frontier molecular orbitals and the electronic band gaps are mutually compared together with the adiabatic electronic intramolecular reorganization energies. The influence of the molecular structure on the calculated quantities was discussed and the effect of chemical modification was shown.

Acknowledgment

The work has been supported by Slovak Grant Agency (1/0601/15) and Slovak Research and Development

Agency (APVV-15-0079). We are grateful to the HPC center at the Slovak University of Technology in Bratislava, which is a part of the Slovak Infrastructure of High Performance Computing (SIVVP project, ITMS code 26230120002, funded by the European region development funds, ERDF) for the computational time and resources made available.

References

Becke AD (1988) Density-functional exchange-energy approximation with correct asymptotic behavior. Phys. Rev. A 38: 3098—3100.

Beu T, Onoe J, Hida A (2005) First-principles calculations of the electronic structure of one-dimensional C60 polymers. Phys. Rev. B 72: 155416.

Brédas J-L, Beljonne D, Coropceanu V, Cornil J (2004) Charge-transfer and energy-transfer processes in pi-conjugated oligomers and polymers: a molecular picture. Chem. Rev. 104 (11): 4971.

Brütting W (2005) Organic Semiconductors. University of Augsburg, Germany.

Cornill J, Brédas J-L, Zaumseil J, Sirringhaus H (2007) Ambipolar transport in organic conjugated materials. Adv. Mat. 19 (14): 1791—1799.

Filo J, Putala M (2010) Semiconducting organic molecular materials. Journal of Electrical Engineering, Vol. 61, No. 5: 314—320.

Flukiger P, Luthi HP, Sortmann S, Weber J (2002) Molekel 4.3, Swiss NationalSupercomputing Centre, Manno, Switzerland.

Frisch MJ, Trucks GW, Schlegel HB, Scuseria GE, Robb MA, Cheeseman JR, Scalmani G, Barone V, Mennucci B, Petersson GA, Nakatsuji H, Caricato M, Li X, Hratchian HP, Izmaylov AF, Bloino J, Zheng G, Sonnenberg JL, Hada M, Ehara M, Toyota K, Fukuda R, Hasegawa J, Ishida M, Nakajima T, Honda Y, Kitao O, Nakai H, Vreven T, Montgomery Jr. JA, Peralta JE, Ogliaro F, Bearpark M, Heyd JJ, Brothers E, Kudin KN, Staroverov VN, Keith T, Kobayashi R, Normand J, Raghavachari K, Rendell A, Burant JC, Iyengar SS, Tomasi J, Cossi M, Rega N, Millam JM, Klene M, Knox JE, Cross JB, Bakken V, Adamo C, Jaramillo J, Gomperts R, Stratmann RE, Yazyev O, Austin AJ, Cammi R, Pomelli C, Ochterski JW, Martin RL, Morokuma K, Zakrzewski VG, Voth GA, Salvador P, Dannenberg JJ, Dapprich S, Daniels AD, Farkas O, Foresman JB, Ortiz JV, Cioslowski J, Fox DJ (2010) Gaussian 09 Revision C.01, Gaussian, Inc., Wallingford, CT.

Hariharan PC, Pople JA (1973) The Influence of Polarization Functions on Molecular Orbital Hydrogenation Energies. Theoret. Chimica Acta 28: 213—222.

Hohenberg P, Kohn W (1964) Inhomogeneous electron gas. Phys. Rev. 136: B864—B871.

Lee C, Yang W, Parr RG (1988) Development of the Colle-Salvetti correlation-energy formula into a functional of the electron density, Phys. Rev. B 37: 785—789.

Marcus RA (1993) Electron transfer reactions in chemistry. Theory and experiment. Rev. Mod. Phys. 65: 599.

McCormick TM, Bridges CR, Carrera EI, DiCarmine PM, Gibson GL, Hollinger J, Kozycz LM, Seferos DS (2013) Conjugated Polymers: Evaluating DFT Methods for More Accurate Orbital Energy Modeling. Macromolecules 46: 3879—3886.

Norton JE, Brédas J-L (2008) Polarization energies in oligoacene semiconductor crystals. J. Am. Chem. Soc. 130 (37): 12377—84.

Olivier Y, Lemaur V, Bredas J-L, Cornil J (2006) Charge Hopping in Organic Semiconductors: Influence of Molecular Parameters on Macroscopic Mobilities in Model One-Dimensional Stacks. J. Phys. Chem. A 110 (19): 6356.

Rassolov V, Pople JA, Ratner M, Windus TL (1998) 6–31G* basis set for atoms K through Zn. J. Chem. Phys. 109: 1223—1229.

Reiss P, Couderc E, De Girolamo J, Pron A (2011) Conjugated polymers/semiconductor nanocrystals hybrid materials—preparation, electrical transport properties and applications. Nanoscale 3: 446—489.

Runge E, Gross EKU (1984) Density-Functional Theory for Time-Dependent Systems. Phys. Rev. Lett. 52: 997—1000.

Sawadogo R, Diendéré F, Guiguemdé I, Ouédraogo R, Sotiropoulos J-M (2016) Semiconducting Oligomers of 1,4-dimethoxybenzene, Thiophene and Thiazole: A Theoretical Study. ACSJ 17(1): 1—10.

Sigma Aldrich (2017) Available on internet: http://www.sigmaaldrich.com/.

Wang L, Li P, Xu B, Zhang H, Tian W (2014) The substituent effect on charge transport property of triisopropylsilylethynyl anthracene derivatives. Org. Electron. 15: 2476—2485.

Yin SW, Yi YP, Li QX, Yu G, Liu YG, Shuai YG (2006) Balanced Carrier Transports of Electrons and Holes in Silole-Based Compounds. A Theoretical Study. J. Phys. Chem. A. 110: 7138.

Zahn DRT, Gavrila GN, Gorgoi M (2006) The transport gap of organic semiconductors studied using the combination of direct and inverse photoemission. Chem. Phys. 325 (1): 99—112.

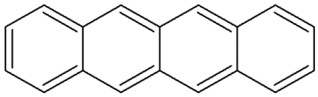

I-p
CAS no. 92-24-0
Benz[b]anthracene

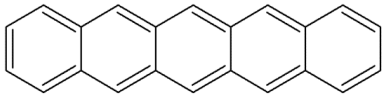

II-p
CAS no. 135-48-8
Pentacene

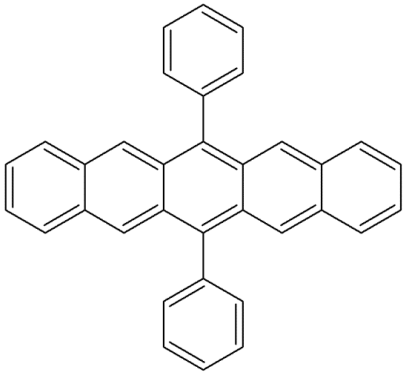

III-p
CAS no. 76727-11-2
6,13-Diphenylpentacene

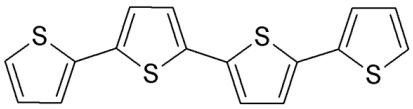

IV-p
CAS no. 5632-29-1
2,2':5',2":5",2"'-Quaterthiophene

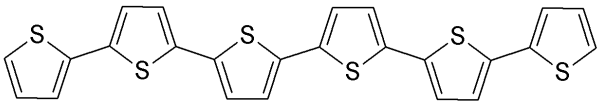

V-p
CAS no. 88493-55-4
α-Sexithiophene

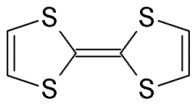

VI-p
CAS no. 31366-25-3
Tetrathiafulvalene

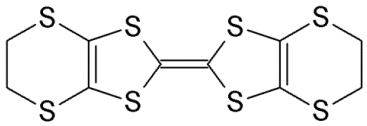

VII-p
CAS no. 66946-48-3
Bis(ethylenedithio)tetrathiafulvalene

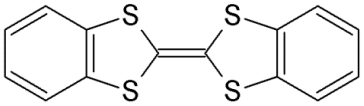

VIII-p
CAS no. 2648-13-3
Dibenzotetrathiafulvalene

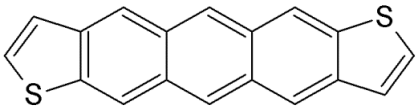

IX-p
CAS no. 144413-58-1
Anthra[2,3-b:6,7-b']dithiophene

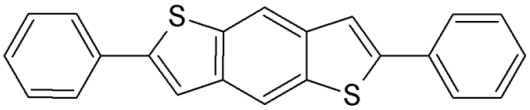

X-p
CAS no. 219597-02-1
2,6-Diphenylbenzo [1,2-b:4,5-b']dithiophene

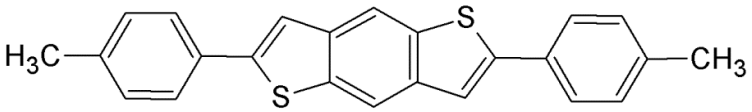

XI-p
CAS no. 1134942-20-3
2,6-Ditolylbenzo[1,2-b:4,5-b']dithiophene

Fig. 1. Schematic structure of selected p-semiconducting organic molecules.

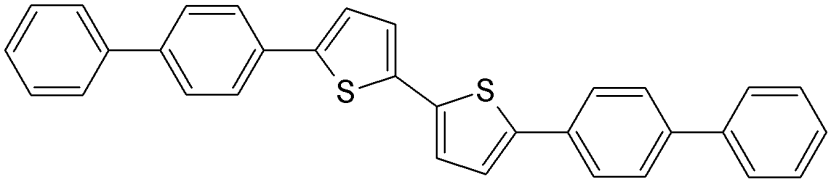

XII-p
CAS no. 175850-28-9
5,5'-Di(4-biphenylyl)-2,2'-bithiophene

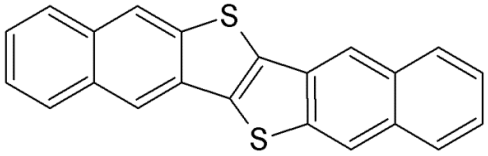

XIII-p
CAS no. 935280-42-5
Dinaphtho[2,3-b:2',3'-f]thieno [3,2-b] thiophene

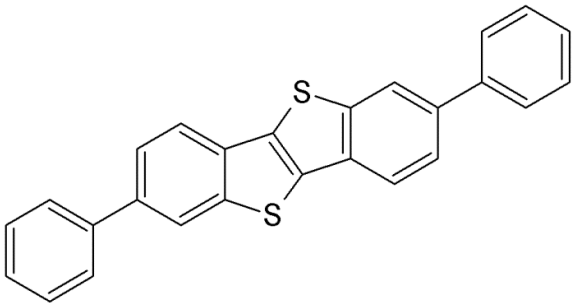

XIV-p
CAS no. 900806-58-8
2,7-Diphenyl[1]benzothieno [3,2-b][1]benzothiophene

Fig. 1 (continued). Schematic structure of selected p-semiconducting organic molecules.

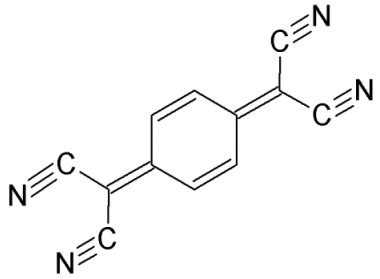

I-n
CAS no. 1518-16-7
7,7,8,8-Tetracyanoquinodimethane

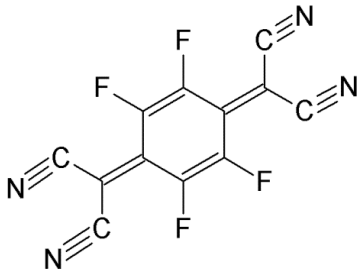

II-n
CAS no. 29261-33-4
2,3,5,6-Tetrafluoro-7,7,8,8-tetracyanoquinodimethane

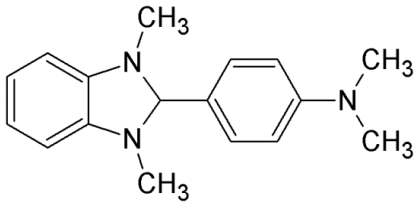

III-n
CAS no. 302818-73-1
4-(2,3-Dihydro-1,3-dimethyl-1H-benzimidazol-2-yl)-N,N-dimethylbenzenamine

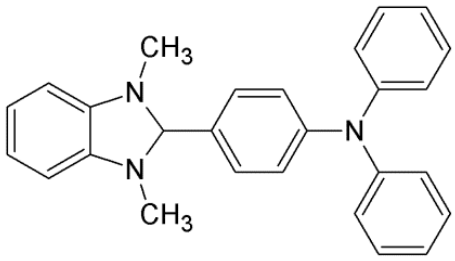

IV-n
CAS no. Not available
4-(1,3-Dimethyl-2,3-dihydro-1H-benzoimidazol-2-yl)-N,N-diphenylaniline

Fig. 2. Schematic structure of selected n-semiconducting organic molecules.

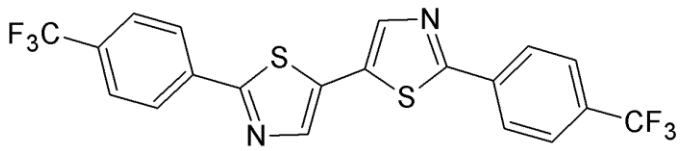

V-n
CAS no.869896-76-4
2,2'-Bis[4-(trifluoromethyl)phenyl]-5,5'-bithiazole

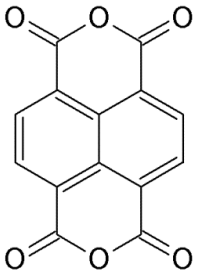

VI-n
CAS no. 81-30-1
1,4,5,8-Naphthalenetetracarboxylic dianhydride

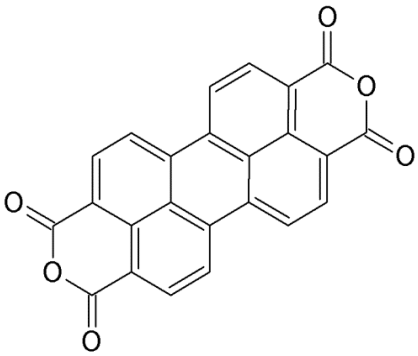

VII-n
CAS no. 128-69-8
Perylene-3,4,9,10-tetracarboxylic dianhydride

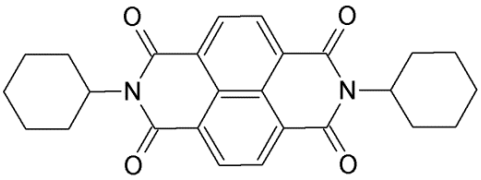

VIII-n
CAS no. 173409-43-3
1,3,6,8(2H,7H)-Tetraone, 2,7-dicyclohexylbenzo[lmn][3,8]phenanthroline

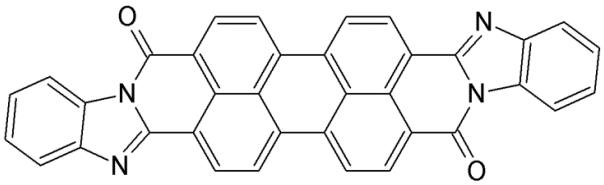

IX-n
CAS no. 55034-79-2
Bisbenzimidazo[2,1-a:2',1'-a']anthra[2,1,9-def:6,5,10-d'e'f']diisoquinoline-10,21-dione

Fig. 2 (continued). Schematic structure of selected n-semiconducting organic molecules.

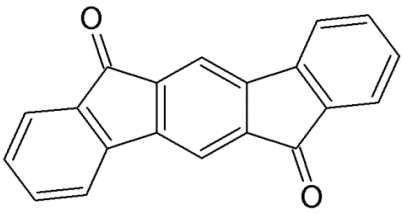

X-n
CAS no. 5695-13-6
Indeno[1,2-b]fluorene-6,12-dione

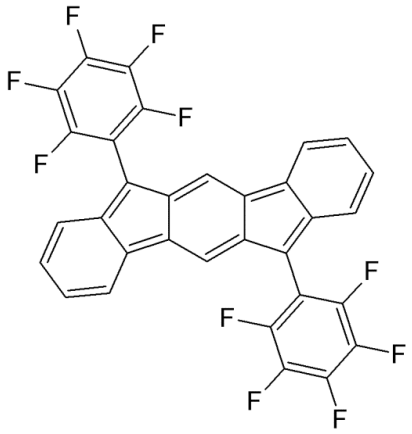

XI-n
CAS no. 1382350-89-1
6,12-Bis(2,3,4,5,6-pentafluorophenyl)
indeno[1,2-b]fluorene

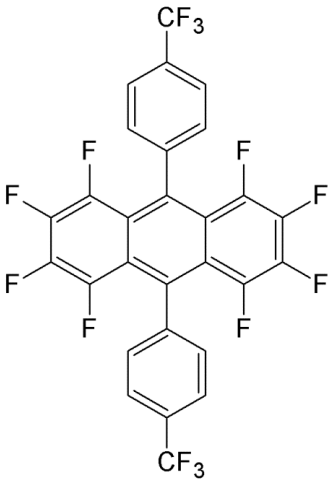

XII-n
CAS no. 1067426-44-1
1,2,3,4,5,6,7,8-Octafluoro-9,10-bis
[4-(trifluoromethyl)phenyl]anthracene

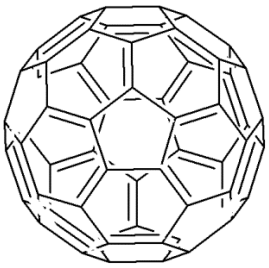

XIII-n
CAS no. 996685-96-8
Fulerene C60

Fig. 2 (continued). Schematic structure of selected n-semiconducting organic molecules.

Molecule III-p

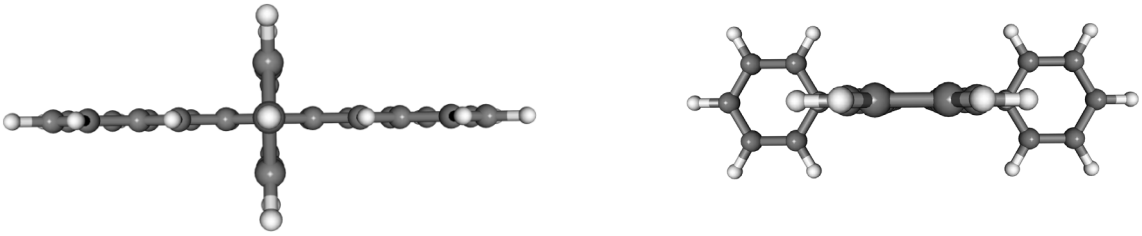

Side view | Front view

Molecule X-p

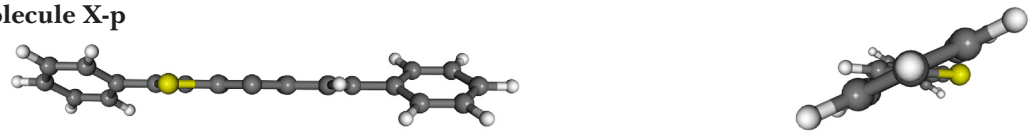

Side view | Front view

Molecule XII-p

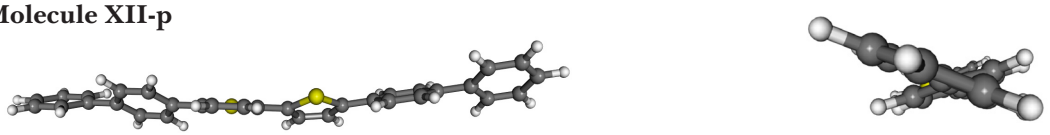

Side view | Front view

Molecule IV-n

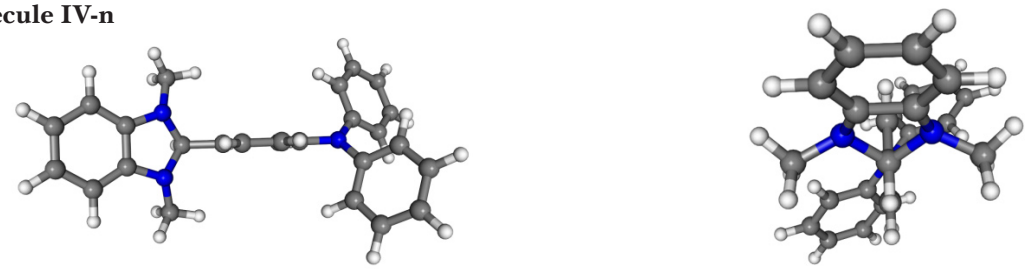

Side view | Front view

Molecule V-n

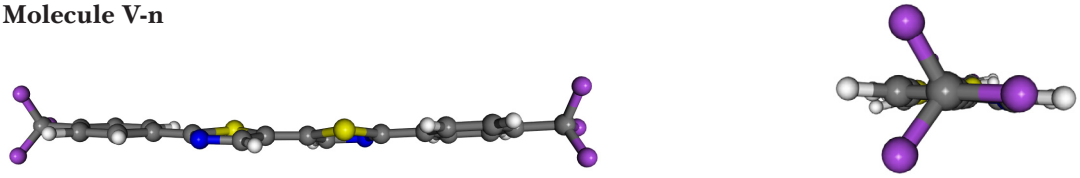

Side view | Front view

Fig. 3. The side and front views of **III-p**, **XII-n**, **IV-n**, **VIII-n** and **XI-n** molecules. Atom colour notation is: grey – carbon, white – hydrogen, yellow – sulphur, blue – nitrogen, red – oxygen and purple – fluorine.

Molecule VIII-n

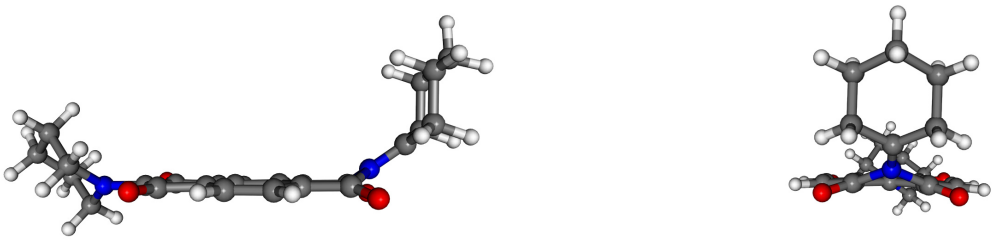

Side view Front view

Molecule XI-n

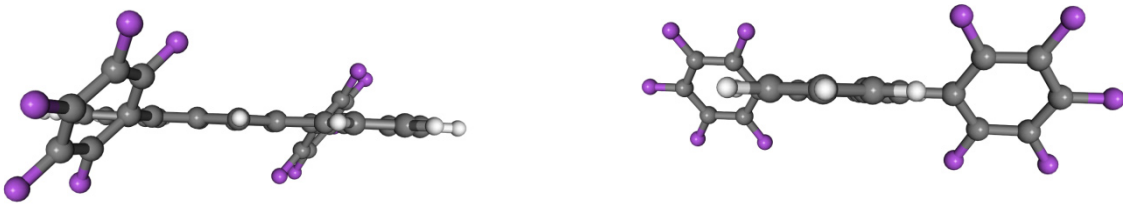

Side view Front view

Molecule XII-n

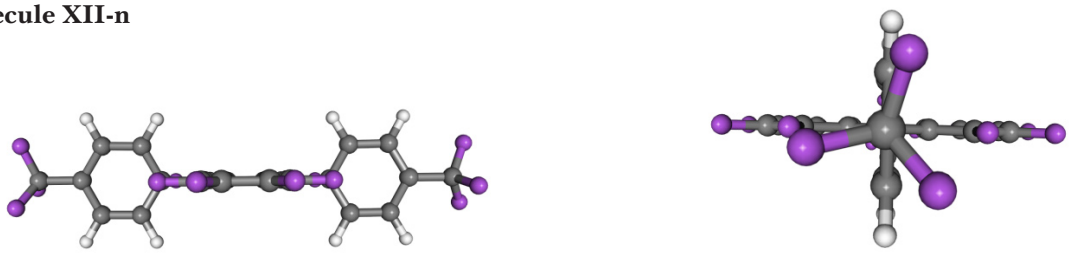

Side view Front view

Fig. 3 (continued). The side and front views of **III-p**, **IV-n**, **VIII-n, XI-n** and **XII-n** molecules. Atom colour notation is: grey — carbon, white — hydrogen, yellow — sulphur, blue — nitrogen, red — oxygen and purple — fluorine.

Tab. 1. The DFT-B3LYP calculated relaxation energies ($\lambda^{\pm}_{1/2}$) and reorganization energies $\lambda^{\pm}$ (in eV) for studied molecules.

p-type	λ_1^+	λ_2^+	λ^+	n-type	λ_1^-	λ_2^-	λ^-
I-p	0.060	0.059	0.119	**I-n**	0.138	0.130	0.269
II-p	0.051	0.049	0.101	**II-n**	0.143	0.132	0.274
III-p	0.061	0.071	0.133	**III-n**	0.378	0.406	0.784
IV-p	0.238	0.167	0.405	**IV-n**	0.189	0.230	0.419
V-p	0.207	0.153	0.360	**V-n**	0.178	0.165	0.344
VI-p	0.143	0.143	0.286	**VI-n**	0.354	0.167	0.521
VII-p	0.278	0.235	0.513	**VII-n**	0.131	0.130	0.261
VIII-p	0.126	0.131	0.257	**VIII-n**	0.838	0.519	1.357
IX-p	0.049	0.050	0.099	**IX-n**	0.119	0.109	0.228
X-p	0.158	0.147	0.304	**X-n**	0.150	0.153	0.303
XI-p	0.153	0.149	0.302	**XI-n**	0.148	0.135	0.283
XII-p	0.199	0.154	0.354	**XII-n**	0.171	0.168	0.340
XIII-p	0.066	0.068	0.134	**XIII-n**	0.068	0.067	1.352
XIV-p	0.123	0.118	0.241				

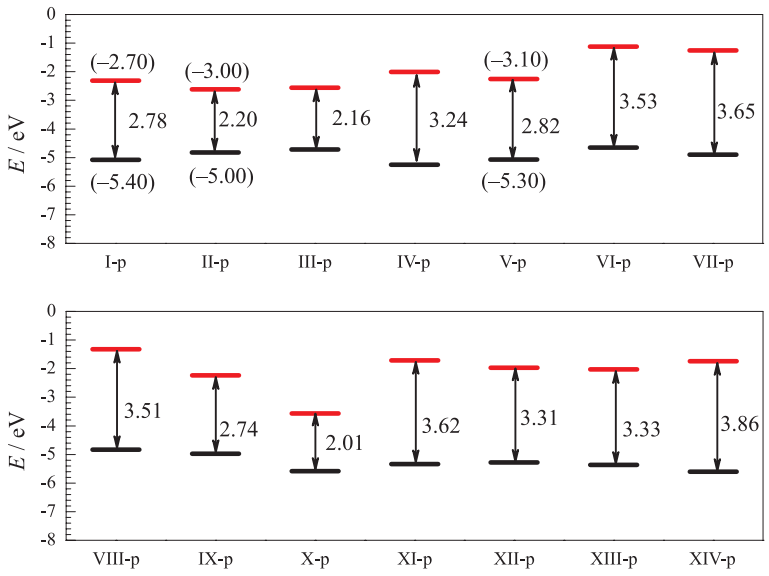

(a)

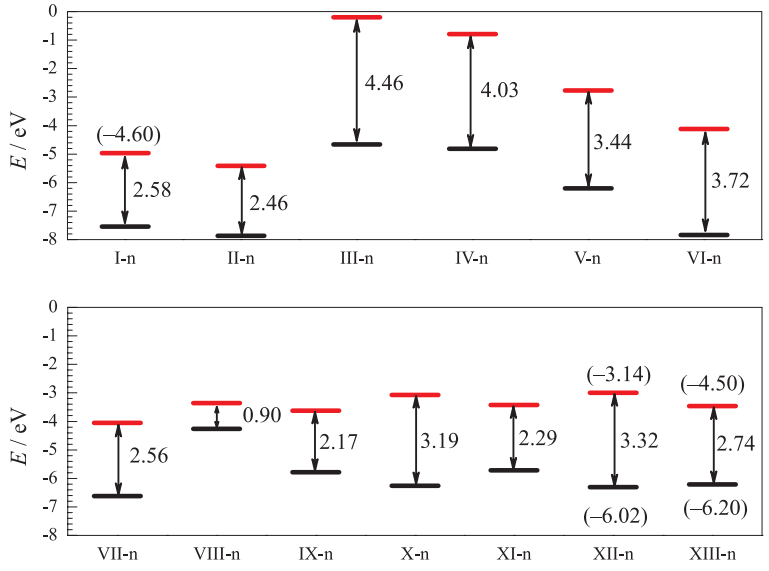

(b)

Fig. 4. Energy diagram of B3LYP frontier molecular orbitals and corresponding energy gaps for selected p-semiconducting (a) and n-semiconducting (b) organic molecules. The experimental values (Sigma Aldrich, 2017) are written in eV in parentheses.